ICAS 2020 SHANG HAI
International Council of the Aeronautical Sciences
32nd Congress of the International Council of the Aeronautical Sciences
September 6-10, 2021
Pudong Shangri-La, Shanghai, China

LANDING SYSTEM USING EXTENDED DYNAMIC WINDOW APPROACH FOR FIXED-WING UAV

Shotaro Ishioka[1], Kenji Uchiyama[1] & Kai Masuda[1]

[1]Department of Aerospace Engineering, Nihon University, Japan

Abstract

We have developed an autonomous landing system that considers some restrictions of the fixed-wing UAV. The control inputs may become a massive value to go along the landing trajectory that is designed before landing if the attitude of the UAV is disturbed by external disturbances. However, the control inputs of a fixed-wing UAV have saturations. Therefore, the landing guidance method should consider the constraints of the control inputs and the state variables. In the proposed method, The dynamic window approach (DWA) that considers some restrictions on velocity space is applied to the landing mission of a fixed-wing UAV. However, some problems arise when applying DWA to a UAV because DWA was developed for ground vehicles. In this paper, we propose the extended DWA that solves the problems in order to apply to a fixed-wing UAV. The numerical simulations are carried out to confirm the validity of the proposed method.

Keywords: Dynamic Window Approach, Optimization Problem, Fixed-Wing UAV, Automatic Landing

1. Introduction

An unmanned aerial vehicle (UAV) is utilized for various situations such as disaster investigation, aerial photography, delivery, and so on. In recent years, a UAV is sold inexpensively and available on the market for domestic use. Therefore, anyone can purchase it for aerial photography. A UAV has various types all over the world. Many companies and institutes have developed a fixed-wing UAV, a multi-copter, an ornithopter, and a tilt-wing UAV. Among these UAVs, a multi-copter is especially famous. A multi-copter does not need a flight strip because it can vertically take off and land on the ground to ensure high safety. Moreover, everyone can operate intuitively because the structure of a multi-copter is straightforward. For example, Amazon uses a multi-copter that has six propellers for delivery. A multi-copter is also utilized for aerial photography and pesticide spraying. However, it has a problem which is a short flight range because it is necessary to keep giving thrust force for supporting its weight. On the other hand, a fixed-wing UAV is also focused by many researchers. It does not require to keep giving thrust force during steady flight because it has gliding capacity. Therefore, it has excellent energy efficiency and is suited for delivery to a remote location. However, a fixed-wing UAV requires an airport with a long flight strip because it cannot vertically take off and land on the ground. Moreover, It is difficult to land automatically for a fixed-wing UAV. A tilt-rotor UAV that can change the direction of the rotor has developed. It can vertically take off and land on the ground. A tilt-wing UAV that can rotate the wing can take off and land on the ground vertically, too. Their flight range is long because these UAVs have some fixed wings. However, it is difficult to control the UAVs because the structures of these UAVs are incredively complicated. Moreover, the probability of fault is high because they have many machine components. Therefore, there are advantages and disadvantages according to each type of UAV. In this paper, the autonomous landing system of a fixed-wing UAV is focused.

Recently, a multi-copter has developed rapidly, and many pieces of research of a multi-copter landing system are reported. As shown in reference [1], the authors proposed the design of their landing pad and the detection algorithm based on the vision for estimating the 3D position of the multi-copter. The proposed method is verified the effectiveness by practical experiments. Wenzel et al. [2] develop the system in which the multi-copter tracks the moving ground vehicle while keeping

a constant distance. The visual tracking method that is proposed has a Wii remote infrared camera as the primary sensor. In reference [3], the autonomous landing system that controls the multi-copter for landing at the moving platform is proposed. The proposed method tracks the platform in 2D image space, and the sliding mode controller obtains the command of the velocity. Some researchers also investigate the landing system of a helicopter. Reference [4] proposed the method of vision-based safety navigation and landing. In this method, the waypoint and the landing point are appointed using aerial or satellite images. The landing guidance method of a fixed-wing UAV is not satisfactory in comparison with a multi-copter. However, it has been studied since long ago. The proposed method in reference [5] designs the longitudinal and lateral controllers while landing. The fixed-wing UAV tracks the landing trajectory drawn by the glide path and the flare trajectory (G&F). It is not eacy to design a robust control system with both tracking ability and robustness generally. However, the authors in reference [6] proposed the method which has both abilities. The fixed-wing UAV is controlled by mixed H_2 and H_∞ to track the trajectory designed by G&F. Khan et al., [7] propose the system that changes the automatic landing sequence if the pilot cannot hold correspondence with the UAV. The landing trajectory of a fixed-wing UAV is designed by G&F generally. However, it has some problems. It is necessary to design the trajectory before landing. As a result, the attitude of the fixed-wing UAV is suddenly changed for tracking the designed trajectory if the UAV positions close to the landing point. The controller gains should be tuned separately for each trajectory because the landing trajectory changes from the glide to the flare trajectory.

The above problems can be solved by considering the restrictions of the state variables. Model predictive control (MPC) is utilized because MPC can consider some restrictions. In reference [8], the proposed method uses MPC as a longitudinal controller. The flight path angle is controlled for tracking the trajectory obtained by G&F. The fixed-wing UAV in reference [9] is reached at the landing point by nonlinear MPC. The UAV can land with stability in a deep stall because the controller considers the restrictions of the state variables. However, MPC needs a heavy calculation load for obtaining the command value for landing. Therefore, a method that has a low calculation load for designing the landing trajectory is needed.

Fox et al., [10] developed Dynamic Window Approach (DWA) that considers the restrictions for guide robot which moves on the ground. DWA considers the restrictions using some windows that are defined on velocity space. The restrictions are defined by the robot's velocity, angular velocity, acceleration, and angular acceleration. The guide robot can reach the target point without colliding obstacles using DWA. This paper deal with the landing problem of a fixed-wing UAV. The function of DWA should be extended for applying to a fixed-wing UAV because the proposed method handles many problems while landing.

We improve DWA for applying to the landing problem of a fixed-wing UAV. The system of the UAV has high nonlinearity when the variation of the attitude becomes a large value. Therefore, this paper does not design the linear controller but the nonlinear controller. The controller consists of the dynamic inversion (DI) method and Linear Quadratic Regulator. The proposed method called the extended DWA (EDWA) is compared with the conventional DWA concerning the calculation load. Moreover, the proposed method will be verified to be superior to G&F by the numerical simulations.

2. Equation of Motion of Fixed-Wing UAV

Figure 1 shows the inertial coordinate system and body-fixed coordinate system of a fixed-wing UAV. In this paper, the fixed-wing UAV has a propeller thrust, and three steering angles the aileron, the elevator, and the rudder. Thus, the fixed-wing UAV is controlled by the thrust and three steering angles. The propeller thrust generates propulsion, and the steering angles give moments to the fixed-wing UAV for trimming the attitude.

Nonlinear equations describe the system of most robots. The system of a fixed-wing UAV, which is not an exception, is expressed by them. The equation of motion of a fixed-wing UAV is divided into translational motion and rotational motion. The translational motion of a fixed-wing UAV is represented by

$$\dot{\mathbf{V}}=-\tilde{\boldsymbol{\omega}}\mathbf{V}+\mathbf{C}^{B/I}\mathbf{g}+\frac{1}{m}\left(\mathbf{C}^{B/W}\mathbf{F}+\mathbf{T}\right) \tag{1}$$

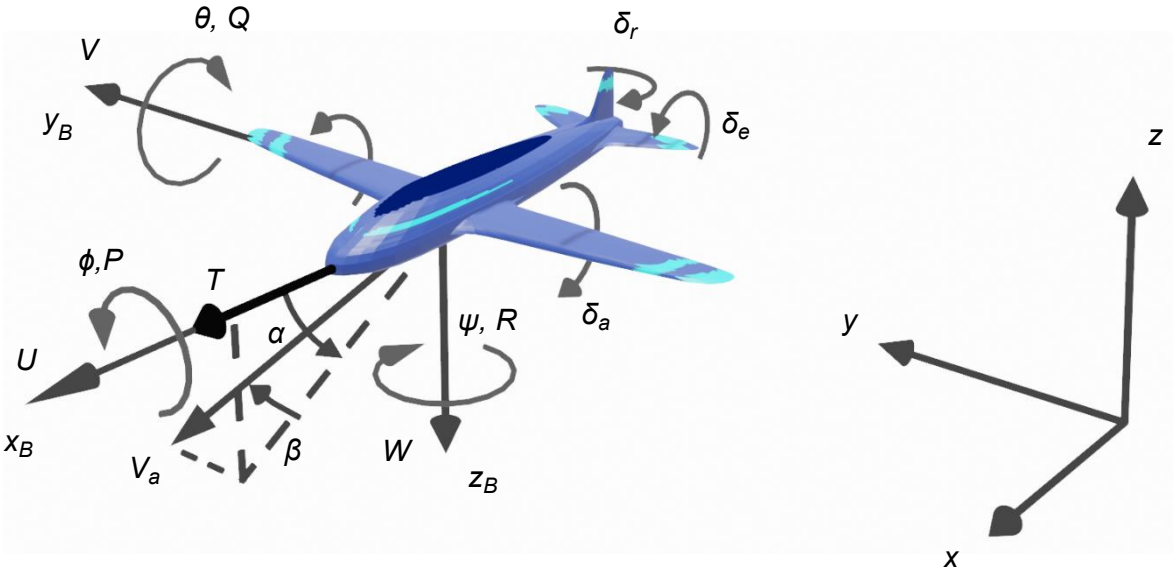

Body-fixed coordinate system Inertial coordinate system

Figure 1 – Coordinate systems and state variables.

where **V** and **ω** are velocity vector and angular velocity vector of the UAV in the body-fixed coordinate system, $\tilde{\boldsymbol{\omega}}$ skew-symmetric matrix, $\mathbf{C}^{B/I}$ coordinate transform matrix obtained by Euler angle of the UAV's attitude from the inertial coordinate system to the body-fixed coordinate system, **g** gravitational acceleration vector, *m* mass of the UAV, $\mathbf{C}^{B/W}$ coordinate transform matrix from the wind axis system to the body-fixed coordinate system, **F** air force vector acting on the UAV, **T** thrust vector generated by the propeller thrust.
The rotational motion of a fixed-wing UAV is given as

$$\dot{\boldsymbol{\omega}}=-\mathbf{J}^{-1}\tilde{\boldsymbol{\omega}}\mathbf{J}\boldsymbol{\omega}+\mathbf{J}^{-1}\mathbf{M}+\mathbf{J}^{-1}\mathbf{M}_u\mathbf{u} \tag{2}$$

where **J** denotes the moment of inertia around the mass center of the UAV, **M** moment acting on the UAV by the air force, $\mathbf{M}_u$ moment acting on the UAV by the three steering angles, **u** control inputs vector. The navigation function that transforms from the velocity vector to the position of the UAV is shown as

$$\dot{\mathbf{X}}=\mathbf{C}^{I/B}\mathbf{V} \tag{3}$$

where **X** represents the position of the UAV in the inertial coordinate system, $\mathbf{C}^{I/B}$ coordinate transform matrix from the body-fixes coordinate system to the inertial coordinate system. The following equation calculates $\mathbf{C}^{I/B}$.

$$\mathbf{C}^{I/B}=\begin{bmatrix}\cos\psi\cos\theta & \cos\psi\sin\theta\sin\phi-\sin\psi\cos\phi & \cos\psi\sin\theta\cos\phi+\sin\psi\sin\phi\\ \sin\psi\cos\theta & \sin\psi\sin\theta\sin\phi+\cos\psi\cos\phi & \sin\psi\sin\theta\cos\phi-\cos\psi\sin\phi\\ -\sin\theta & \cos\theta\sin\phi & \cos\theta\cos\phi\end{bmatrix} \tag{4}$$

The kinematic equation that obtains the attitude of the UAV using the angular velocity vector is shown as

$$\dot{\boldsymbol{\Theta}}=\boldsymbol{\pi}(\boldsymbol{\Theta})\boldsymbol{\omega} \tag{5}$$

where **Θ** expresses the attitude of the UAV by Euler angle in the inertial coordinate system, **π(Θ)** transformation matrix that transforms the angular velocity vector to the attitude of the UAV. **π(Θ)** is denoted by

$$\boldsymbol{\pi}(\boldsymbol{\Theta})=\begin{bmatrix} 1 & \sin\phi\tan\theta & \cos\phi\tan\theta \\ 0 & \cos\phi & -\sin\phi \\ 0 & \sin\phi/\cos\theta & \cos\phi/\cos\theta \end{bmatrix} \tag{6}$$

The air force vector **F** in equation (1) is expressed in the numerical simulation. However, the numerical simulation cannot calculate it exactly; therefore, it is assumed the linear against state variables of the UAV.

A fixed-wing UAV has a unique characteristic called the back-side region. This characteristic causes reversion of the flight characteristic. It is necessary to consider the back-side region because it affects control performance seriously.

The flight path angle of the UAV is obtained by

$$\gamma=\theta-\alpha \tag{7}$$

If the motion of the UAV is linear against its state variables, the transfer functions from the elevator δ_e to the attack angle α and the pitch angle θ are shown as following equations [11].

$$\frac{\alpha}{\delta_e}=M_{\delta_e}\frac{s^2-X_u s-(g/U_s)Z_u}{s^4+a_3s^3+a_2s^2+a_1s+a_0} \tag{8}$$

$$\frac{\theta}{\delta_e}=M_{\delta_e}\frac{s^2-(X_u+Z_w)s+X_uZ_w-X_wZ_u}{s^4+a_3s^3+a_2s^2+a_1s+a_0} \tag{9}$$

where X_u, X_w, Z_u, Z_w, and M_{δ_e} mean stability derivatives, g gravitational acceleration, U_s horizontal steady flight velocity on the x-axis in the body-fixed coordinate system, a_i (i=0, 1, 2, 3) constant coefficients obtained by stability derivatives, s complex number.

The transfer function from the elevator to the flight path angle is calculated by equations (7), (8), and (9).

$$\frac{\gamma}{\delta_e}=-M_{\delta_e}Z_w\frac{s+b_\gamma}{s^4+a_3s^3+a_2s^2+a_1s+a_0} \tag{10}$$

where b_γ is called the back-side parameter. Moreover, the transfer function from the elevator to the small disturbance velocity on the x-axis in the body-fixed coordinate system u is denoted by

$$\frac{u}{\delta_e}=M_{\delta_e}\frac{(U_sX_w-g)s-Z_wg}{s^4+a_3s^3+a_2s^2+a_1s+a_0} \tag{11}$$

The transfer function from small disturbance velocity in the x-axis to the flight path angle is calculated by equations (10) and (11).

$$\frac{\gamma}{u}=\frac{-Z_w(s+b_\gamma)}{(U_sX_w-g)s+gZ_w} \tag{12}$$

The above equation is substituted in the final value theorem.

$$\left(\frac{\gamma}{u}\right)_{ss}=-\frac{b_\gamma}{g} \tag{13}$$

If the calculation result of equation (13) is a negative value, the zero-point of the transfer function is located left half-plane. Therefore, given that throttle is a constant value, and the elevator is actuated negatively, the UAV's velocity declines, and the flight path angle is increased. On the other hand, if the elevator is actuated positively, the velocity is increased, and the flight path angle is decreased. The flight region, like this, is called "the front-side region".

The zero-point of the transfer function in equation (12) is located right half-plane if the back-side parameter is a negative value. In this case, the flight path angle is decreased in the early response

when the elevator is actuated negative angle. The flight region in which the back-side parameter becomes a negative value is called “the back-side region”.
The back-side region can be denoted that relevant to the drag and the velocity. The following equation obtains the drag coefficient C_D.

$$C_D = C_{Dpmin} + \frac{C_L^2}{\pi e AR} \tag{14}$$

where C_{Dpmin} means the minimum parasite drag coefficient, C_L the lift coefficient, e the airplane efficiency, AR the aspect ratio of the main wing. Therefore, the drag D of the UAV is calculated by

$$D = \frac{1}{2}\rho U^2 S\left(C_{Dpmin} + \frac{C_L^2}{\pi e AR}\right) \tag{15}$$

where ρ has defined the atmospheric density, U the velocity of the UAV on the x-axis, S the are of the main wing. The above equation is deformed to the following equation when considering the steady horizontal flight because the lift is equilibrated with gravitational force.

$$D = \frac{1}{2}\rho S C_{Dpmin} U^2 + \frac{2(mg)^2}{\rho S \pi e AR}\frac{1}{U^2} \tag{16}$$

Figure 2, depicted by equation (16), discriminates the front-side and back-side regions.

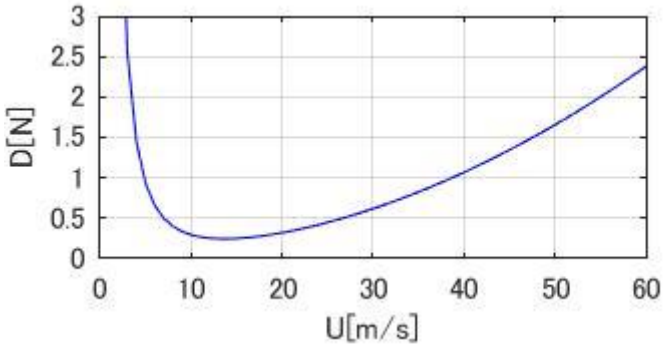

Figure 2 – Back-side region.

The flight region is divided into the front-side region and the back-side region by the velocity at which the gradient of the curve line equals zero. In the front-side region, if the velocity of the UAV is faster than the velocity in the steady flight, the velocity decreased to the steady flight velocity because the drag becomes strong. On the other hand, the velocity cannot return to the steady flight velocity in the back-side region because the drag force increases in the back-side region when the velocity of the UAV is slower than the velocity in the steady flight. Therefore, it is necessary to consider the back-side region to design the guidance or control method. In this paper, the guidance method considers the back-side region.

3. Dynamic Window Approach

3.1 Conventional DWA

DWA is developed for a synchro drive robot by Fox D, Burgard W, and Thrum S in 1996. This method is used for a guide robot in an art museum. The guide robot using DWA considers the restrictions for avoiding some obstacles and people. The way of considering the restrictions is different from a conventional guidance method. In this method, the restrictions are considered with some windows on the velocity space.

3.1.1 Dynamic Window

A robot has some restrictions on velocity, angular velocity, control input, and attitude. For example, in the art museum, it is dangerous that the robot moves quickly. The conventional DWA considers

the restrictions of the velocity, the angular velocity, the acceleration, and the angular acceleration. Figure 3 shows some windows on the velocity space.

Window $\mathbf{V}_s$ which is surrounded by a solid line in figure 3 represents the restriction of the velocity and angular velocity. The following equation defines it.

$$\mathbf{V}_s=\{v,\omega|v_{min}\le v\le v_{max}\cap\omega_{min}\le\omega\le\omega_{max}\} \tag{17}$$

where the subscripts *min* and *max* are denoted lower and upper limit, v the velocity of the robot, ω the angular velocity of the robot. Thus, the acceleration is restricted because the voltage as the control inputs has a limit. The dynamic window $\mathbf{V}_d$ that represents the acceleration constraints in the velocity space is shown by a broken line in figure 3. The dynamic window is also represented below.

$$\mathbf{V}_d=\{v,\omega|v_k-a_{max}T_s\le v\le v_k+a_{max}T_s\cap\omega_k-\Omega_{max}T_s\le\omega\le\omega_k+\Omega_{max}T_s\} \tag{18}$$

The subscript k is the current state variables, T_s the time step interval, a and Ω acceleration, and angular acceleration.

The command of the velocity and angular velocity should be calculated using the distance between the current position and the position of the obstacles to avoid some obstacles. The window $\mathbf{V}_o$ that is designed for avoiding obstacles is obtained by

$$\mathbf{V}_o=\left\{v,\omega|v\le\sqrt{2\cdot dist(v,\omega)\cdot\dot{v}_b}\cap\omega\le\sqrt{2\cdot dist(v,\omega)\cdot\dot{\omega}_b}\right\} \tag{19}$$

where $dist(v,\omega)$ is represented by the distance between the current position and closest obstacle, $\dot{v}_b$ and $\dot{\omega}_b$ accelerations for breakage. The window $\mathbf{V}_o$ is illustrated dash-dot-dash line in figure 3. The window $\mathbf{V}_r$ that is overlapped with the above windows is utilized for considering some restrictions.

$$\mathbf{V}_r=\mathbf{V}_s\cap\mathbf{V}_d\cap\mathbf{V}_o \tag{20}$$

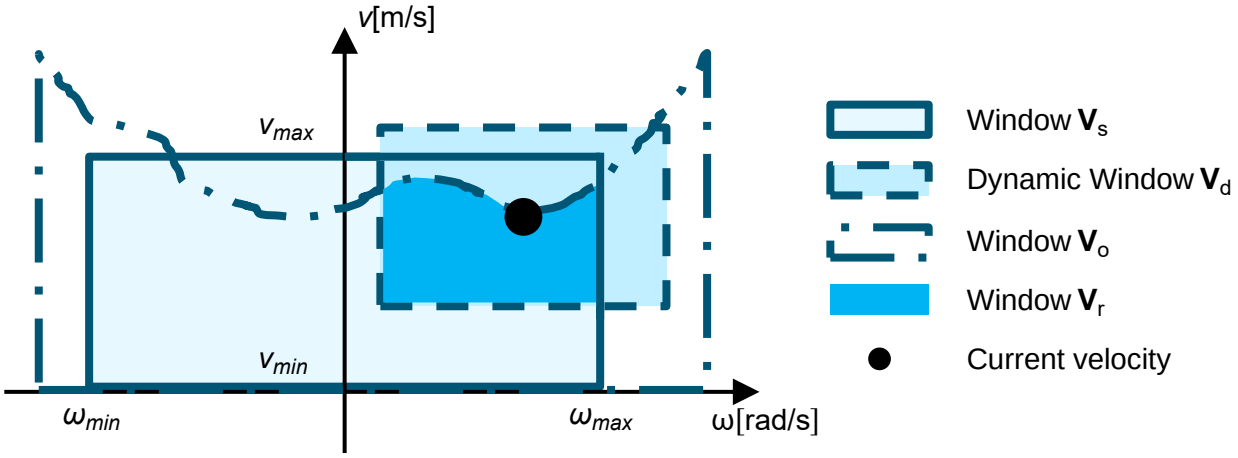

Figure 3 – Principle of the restriction windows.

3.1.2 Evaluation Function

The evaluation function is calculated for choosing the command from window $\mathbf{V}_r$. The evaluation function is defined as below.

$$J=c_1\psi(v,\omega)+c_2d(v,\omega)+c_3v(v,\omega) \tag{21}$$

where c_i ($i=1, 2, 3$) means a constant weighting coefficient. $\psi(v,\omega)$, $d(v,\omega)$ and $v(v,\omega)$ are explained in detail below.

The first term $\psi(v,\omega)$ in equation (21) represents the heading angle of the robot. It becomes a high-performance value when the heading angle faces the direction of the destination. The second term $d(v,\omega)$ is obtained by the position of an obstacle. This term becomes high value when the position of the robot is distant from the closest obstacle. The third term $v(v,\omega)$ is calculated by the absolute

value of the robot's velocity.

The window $\mathbf{V}_r$ is separated in a reticular pattern for calculating the evaluation function. The velocity and the angular velocity at the grid point are utilized. The position of the robot is predicted for calculating every term of the evaluation function.

$$\mathbf{X}_p = \begin{bmatrix} 1 & 0 & 0 & 0 & 0 \\ 0 & 1 & 0 & 0 & 0 \\ 0 & 0 & 1 & 0 & 0 \\ 0 & 0 & 0 & 0 & 0 \\ 0 & 0 & 0 & 0 & 0 \end{bmatrix} \begin{bmatrix} x_p \\ y_p \\ \psi_p \\ v_p \\ \omega_p \end{bmatrix} + \begin{bmatrix} T_s \cos\psi_p & 0 \\ -T_s \sin\psi_p & 0 \\ 0 & T_s \\ 1 & 0 \\ 0 & 1 \end{bmatrix} \begin{bmatrix} v_u \\ \omega_u \end{bmatrix} \tag{21}$$

where the subscript p represents the predicted state variables, the subscript u the candidate for the command value, x and y the position of the robot, ψ the heading angle.

The velocity and the angular velocity that maximize the value of the evaluation function are chosen as a command value. The opted command changes depending on the resolution of the window $\mathbf{V}_r$ and the time step interval.

3.1.3 Defect of Conventional DWA

The conventional DWA is useful for the robot like a car. However, this method has some defects in applying to the landing problem for a fixed-wing UAV. The defects are shown below.

(1) The motion equation of the UAV is not defined in 2-dimensional space but 3-dimensional space.
(2) The attitude is not restricted.
(3) The state variables do not configure the acceleration and the angular acceleration.
(4) The back-side region is not considered.
(5) The method does not judge whether achievable to the target position before going into the motion.
(6) The calculation load is too heavy to calculate the command value online.

3.2 Extended DWA

The proposed method solves the above problems of the conventional DWA.

3.2.1 Evaluation Function

The conventional DWA designs the path for a guidance robot in 2-dimensional space. However, the motion equation of the UAV is denoted by six degrees of freedom flight dynamics. Therefore, extended DWA should design the landing trajectory in 3-dimensional space. In this method, the reference trajectory is utilized to fix the UAV's attitude at the landing point. The attitude at the landing point is significant because of safely landing. The reference trajectory is designed by a sigmoid function as below [12].

$$z_{ref} = \frac{z_0}{1 + exp\left[a_{ref}\left(x - \frac{x_0}{2}\right)\right]} \tag{22}$$

where the subscript 0 indicates the initial value, z_{ref} the altitude of the reference trajectory. a_{ref} is calculated by the margin of the altitude z_d at the landing point.

$$a_{ref} = \frac{2}{x_0} ln \frac{z_d}{z_0 - z_d} \tag{23}$$

The evaluation function is designed to track the above reference trajectory.

$$J = c_1 J_{ref} + c_2 J_g \tag{24}$$

where J_{ref} is obtained by using the reference trajectory.

$$J_{ref} = (z - z_{ref})^2 \tag{25}$$

If the evaluation function has only the first term, the UAV cannot achieve the landing point. Therefore,

the second term that guides the UAV to the landing point is required to reach the target point along the reference trajectory. It is calculated by

$$J_g=x^2+y^2+z^2 \tag{26}$$

In equation (26), the landing point is assumed the original point in the inertia coordinate system. Then, the optimal command value is calculated using the evaluation function in equation (24).

3.2.2 Attitude Restriction

The conventional DWA does not consider the restriction angle. However, it is difficult to continue stable flight if the attitude of the UAV is suddenly changed. Therefore, the attitude has to be restricted in the proposed method. Because windows consider the restrictions in velocity space, the constraint of the angle should also be represented in velocity space. The constraint of the angle $(\zeta_{min}, \zeta_{max})$ is transferred to the angular velocity $(\omega_{ang\text{-}min}, \omega_{ang\text{-}max})$ as below.

$$\begin{aligned}\omega_{ang\text{-}min}&=\frac{\zeta_{min}-\zeta}{T_s}\\ \omega_{ang\text{-}max}&=\frac{\zeta_{max}-\zeta}{T_s}\end{aligned} \tag{27}$$

where ζ is defined as the current angle of the UAV. The above equation is also represented by inequality in velocity space.

$$\mathbf{V}_a=\{v,\ \omega | v_{min}\le v\le v_{max}\cap\omega_{ang\text{-}min}\le\omega\le\omega_{ang\text{-}max}\} \tag{28}$$

3.2.3 Considering Time Delay of Control Input

The conventional DWA considers the restriction of acceleration which is defined by a constant value. However, the acceleration is changed by the current state variables. Therefore, the restriction of the acceleration is calculated using the equation of rotational motion (equation (2)) in the proposed method. Moreover, the time delay of the control inputs is considered as below.
The time delay of the control inputs is represented by the first-order time lag system.

$$\frac{U_a}{U_c}=\frac{K_c}{T_c s+1} \tag{29}$$

where U_a and U_c mean the actual control input and the command voltage that are transformed by Laplace transformation, K_c the regular gain, T_c the time constant. Equation (29) is transformed by inverse Laplace transformation for substituting in equation (2).

$$\dot{u}_a=-\frac{1}{T_c}u_a+K_c u_c \tag{30}$$

where u_a and u_c are obtained by transforming U_a and U_c by inverse Laplace transformation. The acceleration constraint is obtained by setting an arbitrary value to u_c.

3.2.4 Restriction of Back-Side Region

As mentioned in section 2, the back-side region has to be considered for a steady flight. It is necessary to obtain the discriminant of the back-side to define the window of the back-side region constraint. The boundary line between the front-side and the back-side region is represented by the velocity at which the differential value of equation (16) is equal to 0. Therefore, equation (16) is differentiated for the velocity "U". Moreover, it sets to 0 and solves for the velocity "U".

$$U_b^4=\frac{4(mg)^2}{\rho^2 S^2 \pi e A R C_{Dpmin}} \tag{31}$$

The velocity of the UAV does not fall below the velocity U_b using the window in the proposed method.

3.2.5 Possibility of Landing from Initial Position

If the position of the UAV is close to the target point, the UAV should return to the designed trajectory. It is necessary to judge that the UAV can land from the initial position before beginning landing. The gradient of the reference trajectory, which is designed by the sigmoid function, is utilized for judgment. In the case of a steep gradient, the UAV stops to land at the target point. The gradient of the reference trajectory is maximized at the middle point between the initial position and the target point. Therefore, the allowable gradient is configured at an arbitrary angle and substituted in the equation obtained by differentiating the reference trajectory. As a result, the restriction velocity is calculated by solving the equation substituted for the allowable gradient as below.

$$U_j = \frac{xy_0 - \frac{z_0}{2\theta_j} ln \frac{z_0 - z_d}{z_d}}{dt} \tag{32}$$

where xy_0 is obtained by

$$xy_0 = \sqrt{x_0^2 + y_0^2} \tag{33}$$

If the velocity of the UAV is greater than U_j that is calculated by substituting the initial position in equation (32), the UAV cannot land in safety.
Figure 4 shows the restriction windows in the proposed method.

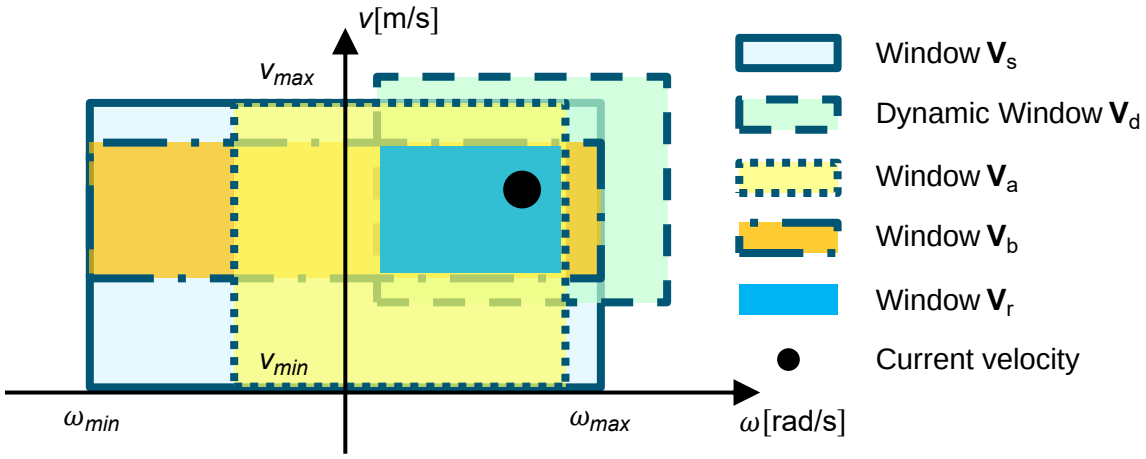

Figure 4 – The restriction windows in the proposed method.

The window $\mathbf{V}_s$ and the window $\mathbf{V}_d$ are defined in equations (17) and (18). Window $\mathbf{V}_a$ represents the restriction angle that is denoted by equation (28). Window $\mathbf{V}_b$ indicates the constraint of the back-side region and the possibility of landing from the initial position. Here, it should be noted that the possibility of landing is considered only at the initial condition. Therefore, the maximum velocity of window $\mathbf{V}_b$ is set in v_{max} at other times. As a result, window $\mathbf{V}_b$ is represented by the following equation in the initial condition.

$$\mathbf{V}_b = \{v, \omega | U_b \le v \le U_j \cap \omega_{min} \le \omega \le \omega_{max}\} \tag{34}$$

In other times,

$$\mathbf{V}_b = \{v, \omega | U_b \le v \le v_{max} \cap \omega_{min} \le \omega \le \omega_{max}\} \tag{35}$$

The proposed method does not need window $\mathbf{V}_o$ in the conventional DWA because there are no obstacles in a flight.

3.2.6 Improvement of Calculation Load

The conventional DWA has the problem of a heavy calculation load. The optimization calculation is utilized for solving this problem.
The following inequalities rewrite window $\mathbf{V}_r$.

$$\begin{aligned} U_{min} \le U \le U_{max} \\ P_{min} \le P \le P_{max} \\ Q_{min} \le Q \le Q_{max} \\ R_{min} \le R \le R_{max} \end{aligned} \tag{36}$$

Because the position of the UAV defines the evaluation function obtained by equation (24), the restrictions in equation (36) should be transformed to the position. They are transformed by using the navigation function and the kinematic function ntegrated by the rectangle formula.

$$\begin{bmatrix} x_{k+1} \\ y_{k+1} \\ z_{k+1} \end{bmatrix} = \begin{bmatrix} x_k \\ y_k \\ z_k \end{bmatrix} + \begin{bmatrix} \cos\psi_{k+1} \cos\theta_{k+1} \\ \sin\psi_{k+1} \cos\theta_{k+1} \\ \sin\theta_{k+1} \end{bmatrix} U_{max/min} T_s \tag{37}$$

$$\begin{bmatrix} \phi_{k+1} \\ \theta_{k+1} \\ \psi_{k+1} \end{bmatrix} = \begin{bmatrix} \phi_k \\ \theta_k \\ \psi_k \end{bmatrix} + \begin{bmatrix} 1 & \sin\phi_k \tan\theta_k & \cos\phi_k \tan\theta_k \\ 0 & \cos\phi_k & -\sin\phi_k \\ 0 & \sin\phi_k / \cos\theta_k & \cos\phi_k / \cos\theta_k \end{bmatrix} \begin{bmatrix} P_{max/min} \\ Q_{max/min} \\ R_{max/min} \end{bmatrix} T_s \tag{38}$$

where k represents the time step. Equation (36) is transformed by substituting equations (37) and (38).

$$\begin{aligned} (x, y, z): \pm(x-x_k)^2 \pm (y-y_k)^2 \pm (z-z_k)^2 \mp (U_{max/min} T_s)^2 \le 0 \\ (x, y, z): \pm y \mp y_k \mp (x-x_k) \tan\psi_{max/min} \le 0 \\ (x, y, z): \pm (z-z_k)^2 \mp \sqrt{(x-x_k)^2 + (y-y_k)^2} \tan\theta_{max/min} \le 0 \end{aligned} \tag{39}$$

where $\theta_{max/min}$ and $\psi_{max/min}$ is determined by the sign of the roll angle ϕ_k as below.
In the case of $\phi_k \geq 0$,

$$\begin{aligned} \psi_{max} = \psi_k + \left(Q_{max} \frac{\sin\phi_k}{\cos\phi_k} + R_{max} \frac{\cos\phi_k}{\cos\theta_k} \right) T_s \\ \psi_{min} = \psi_k + \left(Q_{min} \frac{\sin\phi_k}{\cos\phi_k} + R_{min} \frac{\cos\phi_k}{\cos\theta_k} \right) T_s \\ \theta_{max} = \theta_k + \left(Q_{max} \cos\phi_k - R_{min} \sin\phi_k \right) T_s \\ \theta_{min} = \theta_k + \left(Q_{min} \cos\phi_k - R_{max} \sin\phi_k \right) T_s \end{aligned} \tag{40}$$

In other cases,

$$\begin{aligned} \psi_{max} = \psi_k + \left(Q_{min} \frac{\sin\phi_k}{\cos\phi_k} + R_{max} \frac{\cos\phi_k}{\cos\theta_k} \right) T_s \\ \psi_{min} = \psi_k + \left(Q_{max} \frac{\sin\phi_k}{\cos\phi_k} + R_{min} \frac{\cos\phi_k}{\cos\theta_k} \right) T_s \\ \theta_{max} = \theta_k + \left(Q_{max} \cos\phi_k - R_{max} \sin\phi_k \right) T_s \\ \theta_{min} = \theta_k + \left(Q_{min} \cos\phi_k - R_{min} \sin\phi_k \right) T_s \end{aligned} \tag{41}$$

The position as a command value that satisfies the above restrictions and minimizes the evaluation function is obtained by the conjugate gradient method. The problem of the calculation load is improved by solving the above optimization problem. As a result, the calculation load for obtaining the command value in the proposed method is compared with it in the conventional method as below.

Table 1 – Comparison of the calculation load.

Time step interval T_s [sec]	0.100
Calculation time T_p [sec]	0.028
Calculation time T_5 [sec]	0.018
Calculation time T_{10} [sec]	0.941
Calculation time T_{20} [sec]	380.1

where T_p represents the calculation time in the proposed method, T_i (i=*5, 10, 20*) the calculation time in the conventional method, i the resolution of windows. It is clear from table 1 that the calculation load of the proposed method is lighter than it of the conventional method if the resolution is set to 10 or 20. However, when the resolution is set to 5, the calculation load of the conventional DWA is lighter than it of the Extended DWA. When the initial position of the UAV is $[x, y, z]$=[*-15, 5, 5*] , the command of the proposed method is calculated $[x_c, y_c, z_c]$=[*-13.6, 4.86, 4.86*]. The position command of the conventional method is calculated $[x_c, y_c, z_c]$=[*-13.6, 4.95, 5.06*]. The position command of the proposed method is on the reference trajectory, but the position command of the conventional method is not on the trajectory. Therefore, the proposed method is valid for calculating the command.

4. Flight Control System

The control system for landing the UAV at the target point is the DI method and Linear Quadratic Regulator (LQR). In this paper, the attitude of the UAV is controlled. DI method is utilized for canceling the nonlinear term in the equation of motion. LQR becomes stabilized the system which is linearized by the DI method.

The command of the attitude is calculated by the position command, which is acquired using Extended DWA.

$$\theta_c = \tan^{-1} \frac{z_c - z_k}{\sqrt{(x_c - x_k)^2 + (y_c - y_k)^2}}$$
$$\psi_c = \tan^{-1} \frac{y_c - y_k}{x_c - x_k} \tag{42}$$

where θ_c and ψ_c are the commands of pitch angle and yaw angle. The command of roll angle ϕ_c is set to 0 in this paper.

The error equation is defined as

$$\boldsymbol{\Theta}_e = \boldsymbol{\Theta} - \boldsymbol{\Theta}_c = [\phi - \phi_c \quad \theta - \theta_c \quad \psi - \psi_c]^T \tag{43}$$

Equation (43) is differentiated twice with respect to time.

$$\ddot{\boldsymbol{\Theta}}_e = \dot{\boldsymbol{\pi}}(\boldsymbol{\Theta})\boldsymbol{\omega} + \boldsymbol{\pi}(\boldsymbol{\Theta})\dot{\boldsymbol{\omega}} \tag{44}$$

The equation of rotational motion is substituted in the second term of equation (44).

$$\ddot{\boldsymbol{\Theta}}_e = \dot{\boldsymbol{\pi}}(\boldsymbol{\Theta})\boldsymbol{\omega} - \boldsymbol{\pi}(\boldsymbol{\Theta})\mathbf{J}^{-1}\tilde{\boldsymbol{\omega}}\mathbf{J}\boldsymbol{\omega} + \boldsymbol{\pi}(\boldsymbol{\Theta})\mathbf{J}^{-1}\mathbf{M} + \boldsymbol{\pi}(\boldsymbol{\Theta})\mathbf{J}^{-1}\mathbf{M}_u\mathbf{u} \tag{45}$$

The DI method cancels the nonlinear term in the system. The nonlinear term $\mathbf{z}_r$ in equation (45) is denoted by

$$\mathbf{z}_r = \dot{\boldsymbol{\pi}}(\boldsymbol{\Theta})\boldsymbol{\omega} - \boldsymbol{\pi}(\boldsymbol{\Theta})\mathbf{J}^{-1}\tilde{\boldsymbol{\omega}}\mathbf{J}\boldsymbol{\omega} + \boldsymbol{\pi}(\boldsymbol{\Theta})\mathbf{J}^{-1}\mathbf{M} \tag{46}$$

As a result, equation (45) is represented as below.

$$\ddot{\boldsymbol{\Theta}}_e = \mathbf{z}_r + \boldsymbol{\pi}(\boldsymbol{\Theta})\mathbf{J}^{-1}\mathbf{M}_u\mathbf{u} \tag{47}$$

The control input **u** is designed for canceling the nonlinear term.

$$\mathbf{u}=\mathbf{M}_u^{-1}\mathbf{J}\boldsymbol{\pi}(\boldsymbol{\Theta})^{-1}(-\mathbf{z}_r+\mathbf{v}_l) \tag{48}$$

where $\mathbf{v}_l$ means the linear control input designed by LQR in this paper. The above equation is substituted in equation (47).

$$\ddot{\boldsymbol{\Theta}}_e=\mathbf{v}_l \tag{49}$$

Equation (49) is rewritten by matrix notation.

$$\frac{d}{dt}\begin{bmatrix}\boldsymbol{\Theta}_e\\ \dot{\boldsymbol{\Theta}}_e\end{bmatrix}=\begin{bmatrix}\mathbf{0}_{3\times3} & \mathbf{I}_{3\times3}\\ \mathbf{0}_{3\times3} & \mathbf{0}_{3\times3}\end{bmatrix}+\begin{bmatrix}\mathbf{0}_{3\times3}\\ \mathbf{I}_{3\times3}\end{bmatrix}\mathbf{v}_l \tag{50}$$

5. Numerical Simulation

The numerical simulations are carried out to verify the effectiveness of the proposed method. The proposed method is compared with the conventional method in the numerical simulation. The conventional method of the landing problem designs the trajectory that consists of the glide path and the flare trajectory. It is explained in section 5.1. Section 5.2 explains the configuration of the numerical simulation.

5.1 Glide Path and Flare Trajectory

The glide path is represented by a straight line with a gradient of 3° in general. The flare trajectory is defined by a curve line that smoothly connects the glide path to the target point. It is represented by the exponential function that is obtained by the following equation [13].

$$z_c=z_f\,exp\left(-\frac{t}{\tau_f}\right) \tag{51}$$

where τ_f means the time constant, z_f the altitude of the intersecting point of the glide path and the flare trajectory. z_f is calculated by

$$z_f=\frac{x_f\,sin\,3°}{cos\,3°+a_f} \tag{52}$$

where x_f indicates the location of the glide path transmitter, a_f the period between the start and the end of the flare trajectory.
In the numerical simulation, the UAV is controlled for tracking the above trajectory using the same controller as the proposed method.

5.2 Numerical Simulation Settings

A numerical simulation is utilized for confirming the problem of applying the method to an existing system. Therefore, it is necessary to reproduce the actual circumstances in the numerical simulation faithfully. In the landing problem, the numerical simulation should consider the grand effect and the wind disturbances.
The ground effect is represented by the following predictive equations [14].

$$\begin{aligned}\Delta C_L&=\frac{C_L}{K}\left\{(1-K)+\gamma_g\left[\frac{N}{\left(1+\frac{\tau N C_L}{K}\right)^2}-1\right]\right\}\\ \Delta C_D&=-\frac{\sigma C_L^2}{\pi}\left\{C_D-\left(\frac{\sigma C_L^2}{\pi}\right)\right\}\pi\gamma_g C_L\end{aligned} \tag{53}$$

where ΔC_L and ΔC_D indicate the variation of the lift coefficient and the drag coefficient. K is calculated by the lift curve slope, the aspect ratio of the main wing, and σ. σ and γ_g are represented

by the main wingspan and the altitude. N and τ are calculated by the mean aerodynamic chord (MAC) and the altitude.

The Dryden turbulence model represents the wind disturbance that is considered in the numerical simulation. It is obtained by passing the white noise to the shaping filter.

The parameters of the numerical simulation are shown in the following tables. Table 2 denotes the specification of the fixed-wing UAV, which is used for the numerical simulations. The initial state variables of the UAV are shown in table 3. In this paper, the numerical simulations are carried out in 3 conditions. In Condition 1, the UAV locates a sufficient distance from the target point. The position of the UAV in condition 2 does not have a distance which the conventional method requires for landing. The needfulness of landing possibility is confirmed in condition 3. Therefore, the UAV has located in the position that is judged a possible landing or not in the numerical simulation. Condition 3A assumes that the UAV can land from the initial position. The UAV is located the initial position that is judged an impossible landing in condition 3B. In this condition, the UAV should return to where the UAV can land in the proposed method. However, the function of the landing judgment is turned off in condition 3. Table 4 indicates the constant weighting coefficient of Extended DWA in every condition. The conventional method's parameters for calculating equations (51) and (52) are shown in table 5. The restrictions of the UAV's state variables are denoted in table 6. These restrictions are used for designing the landing trajectory in the proposed method. Table 7 shows the weighting coefficients of LQR. In table 7, 1G and 2G mean that the UAV is on the glide path in conditions 1 and 2, 1F and 2F the UAV is on the flare trajectory, 1P and 2P the proposed method utilized in conditions 1 and 2.

5.3 Numerical Simulation Results

Figures 5 and 6 show the results of the numerical simulations, which are performed when the UAV has a sufficient landing distance. The conventional method is used in figure 5. Figure 5 (a) shows the trajectory of the UAV. It is clear that the UAV lands at the target point. The time histories of the altitude are depicted in figure 5 (b). it shows that the UAV connects to the ground smoothly. Figure 5 (c) shows the time histories of the descent rate. The reference trajectory is switched from the glide path to the flare trajectory at 6.30 sec as shown in figure 5 (c). The attitude, which is illustrated in figure 5 (d), does not suddenly change. However, the attitude is disturbed at switching to the flare trajectory from the glide path. In figures 5 (e) and (f), the moving surfaces and throttle cancel the wind disturbances. The results of the numerical simulation using the proposed method are shown in figure 6. The EDWA draws the reference trajectory designed by the sigmoid function as shown in figure 6 (a). Figure 6 (b) which represents the time histories of the altitude shows that the UAV lands smoothly. It can be seen in figure 6 (d), the attitude of the UAV is not disturbed while landing. The time histories of the moving surfaces and throttle are shown in figures 6 (e) and (f). Thus, the UAV can land safely using the conventional method. However, the EDWA is superior to G&F because the variation of the attitude is small while landing compared to G&F.

The numerical simulations which are performed in condition 2 are drawn in figures 7 and 8. The trajectory using G&F is depicted in figure 7 (a). It shows that the UAV cannot reach the target point because the distance between the initial position and the target point is not sufficient for landing if G&F is used as a guidance method. Figure 7 (b) and (c) represent the time histories of the altitude and the rate of descent of the UAV. It is clear that the UAV crashes because the descent ratio is a large value when the UAV connects to the ground. The attitude suddenly changes as shown in figure 7 (d). The moving surfaces epresented in figure 7 (e) and the throttle llustrated in figure 7 (f) cannot control the UAV for landing. Figure 8 shows the result of the numerical simulation using the EDWA. The trajectory of the UAV which is depicted in figure 8 (a) shows that the UAV reaches the original point in the inertial coordinate system. The UAV lands smoothly as shown in figure 8 (b) that shows the time histories of the altitude. The rate of descent is illustrated in figure 8 (c). The UAV can land safely because the descent rate is -0.150 m/s when the UAV connects to the ground. The attitude, which is shown in figure 8 (d), does not suddenly change despite the short landing distance. Figure 8 (e) and (f) show the time histories of the moving surfaces and throttle. The control inputs are small values because the proposed method considers restrictions of the state variables.

Figures 9 and 10 show the result of the numerical simulation in condition 3. The trajectories of the fixed-wing UAV are depicted in figures 9 (a) and 10 (a). The UAV lands at the target point in each

case. The UAV eventually land at $\mathbf{x}=[-0.323\ 0.0874\ 0.0964]^T$ in case of possible landing. In contrast, the UAV reaches $\mathbf{x}=[-0.712\ 0.236\ 0.1329]^T$ in case of impossible landing. Figures 9 (b) and 10 (b) represent the time histories of the altitude. The UAV smoothly lands at the target point. The descent rate becomes -1.30 m/s when the UAV connects to the ground as shown in figure 9 (c). The time histories of the descent rate in condition 3B are illustrated in figure 10 (c). The rate of descent is -1.96 m/s when the UAV touches the ground. Therefore, when the UAV has a distance of possible landing, the landing impact is alleviated. The time histories of the attitude are shown in figures 9 (d) and 10 (d). In condition 3A, the pitch angle of the UAV is -0.500 rad at a minimum while landing. The minimum pitch angle becomes -0.530 rad while landing in condition 3B. The time histories of the moving surfaces are depicted in figures 9 (e) and 10 (e). Figures 9 (f) and 10 (f) show the time histories of the throttle. The control inputs are not required big values because the restrictions of the state variables and control inputs are considered by the proposed method. From the above, the function of the landing judgment is needed for giving assurance of a safe landing.

Table 2 – Specification of UAV.

Full length L[m]	0.890
Wingspan b[m]	0.930
Wing area S [m^2]	0.188
MAC $\overline{c_a}$ [m]	0.205
Mass m [kg]	0.570

Table 3 – Initial conditions.

Position in condition 1 $\mathbf{x}_0$ [m]	$[-120, 5, 5]^T$
Position in condition 2 $\mathbf{x}_0$ [m]	$[-60, 5, 5]^T$
Position in condition 3A $\mathbf{x}_0$ [m]	$[-15, 5, 5]^T$
Position in condition 3B $\mathbf{x}_0$ [m]	$[-14, 5, 5]^T$
Attitude $\boldsymbol{\Theta_0}$ [rad]	$[0, 0, 0]^T$
Velocity $\mathbf{V_0}$ [m/s]	$[12.5, 0, 0]^T$
Angular velocity $\boldsymbol{\omega_0}$ [rad/s]	$[0, 0, 0]^T$

Table 4 – Parameters of DWA.

Weighting coefficient 1 (c_1, c_2) [-]	(4, 1)
Weighting coefficient 2 (c_1, c_2) [-]	(4, 1)
Weighting coefficient 3A (c_1, c_2) [-]	(2, 1)
Weighting coefficient 3B (c_1, c_2) [-]	(2, 1)

Table 5 – Parameters of G&F.

Glide path transmitter x_f [m]	-10.0
Time constant τ_f [sec]	1.90
Flare period a_f [-]	3.00

Table 6 – Restrictions of variables.

Velocity on X-axis (U_{min}, U_{max}) [m/s]	(0, 20.0)
Angular velocity on X-axis (P_{min}, P_{max}) [rad/s]	(-1.00, 1.00)
Angular velocity on Y-axis (Q_{min}, Q_{max}) [rad/s]	(-1.00, 1.00)
Angular velocity on Z-axis (R_{min}, R_{max}) [rad/s]	(-1.00, 1.00)
Acceleration on X-axis $\dot{U}_{max}$ [m/s^2]	1.00
Attitude on X-axis (ϕ_{min}, ϕ_{max}) [rad]	(-0.262, 0.262)
Attitude on Y-axis (θ_{min}, θ_{max}) [rad]	(-0.524, 0.524)

Table 7 – Parameters of controller.

Weighting coefficient 1G (Q, R) [-]	(diag[1 10 10 1 1 1], diag[1 1 1])
Weighting coefficient 1F (Q, R) [-]	(diag[1 1000 1 10 1000 1], diag[1 1 1])
Weighting coefficient 1P (Q, R) [-]	(diag[5 100 10 1 10 10], diag[1 1 1])
Weighting coefficient 2G (Q, R) [-]	(diag[100 1 1 10 1 1], diag[1 1 1])
Weighting coefficient 2F (Q, R) [-]	(diag[10 1 1 100 1 1], diag[1 1 1])
Weighting coefficient 2P (Q, R) [-]	(diag[5 100 10 1 10 10], diag[1 1 1])
Weighting coefficient 3A (Q, R) [-]	(diag[10 200 70 10 200 50], diag[1 1 1])
Weighting coefficient 3B (Q, R) [-]	(diag[10 200 70 10 200 50], diag[1 1 1])

6. Conclusion

We proposed the landing guidance method to add the function to the conventional DWA for applying the fixed-wing UAV. The conventional DWA is confirmed that its calculation load becomes a large value by the numerical simulation. On the other hand, the proposed method which solves the optimization problem reduces its calculation load. The UAV safely lands at the target point because the landing trajectory considers the many restrictions of the UAV by using the EDWA. Moreover, the function of the landing judgment is confirmed its significance by carrying out the numerical simulation that the UAV locates in the position which is judged possible landing or not. Thus, the numerical simulation confirmed the validity of the EDWA for the landing problem.

DI method and LQR control the attitude of the UAV in this paper. As a result, the velocity of the fixed-wing UAV does not decrease until the UAV reaches the landing point. The UAV should be controlled its position because the EDWA calculates the position command. However, the effectual control method that controls the position of the fixed-wing UAV is not proposed to date. We will develop the control method that controls both translational and rotational motion of the fixed-wing UAV in the future work. Moreover, the demonstration experiment will be conducted to confirm the validity of the method.

7. Copyright Statement

References

[1] Lange S, Sunderhauf N and Protzel P. A vision based onboard approach for landing and position control of an autonomous multirotor UAV in GPS-denied environments. *International Conference on Advanced Robotics*, Germany, pp 1-6, 2009.

[2] Wenzel K E, Masselli A and Zell A. Automatic take off, tracking and landing of a miniature UAV on a moving carrier vehicle. *Journal of Intelligent & Robotic Systems*, Vol. 61, pp 221-238, 2011.

[3] Lee D, Ryan T and Kim H J. Autonomous landing of a VTOL UAV on a moving platform using image-based visual servoing. *International Conference on Robotics and Automation*, USA, pp 971-976, 2012.

[4] Cesetti A, Frontoni E, Mancini A, Zingaretti P and Longhi S. A vision-based guidance system for UAV navigation and safe landing using natural landmarks. *Journal of Intelligent & Robotic Systems*, Vol. 57, pp 233-257, 2010.

[5] Muhammad I S, Ahsun U and Haider A B. Lateral and longitudinal guidance and control design of a UAV in auto landing phase. *International Bhurban Conference on Applied Science & Technology*, Pakistan, pp 162-168, 2009.

[6] Nugroho L. Comparison of classical and modern landing control system for a small unmanned aerial vehicle. *International Conference on Computer, Control, Informatics and Its Applications*, Indonesia, pp 187-192, 2014.

[7] Khan S I, Belal T M and Barman S. Auto landing sequence for an unmanned aerial vehicle at a fixed point. *International Conference on Electrical, Computer and Communication Engineering*, Bangladesh, pp 175-180, 2017.

[8] Gripp J A de Bonfim and Sampaio U P. Automatic landing of a UAV using model predictive control for the surveillance of internal autopilot's controls. *International Conference on Unmanned Aircraft Systems*, USA, pp 1219-1224, 2014.

[9] Mathisen S H, Fossen T I and Johansen T A. Non-linear model predictive control for guidance of a fixed-wing UAV in precision deep stall landing. *International Conference on Unmanned Aircraft Systems*, USA, pp 356-365, 2015.

[10] Fox D, Burgard W and Thrun S. Controlling synchro-drive robots with the dynamic window approach to collision avoidance. *International Conference on Intelligent Robots and System*, Japan, Vol. 3, pp 1280-1287, 1996.

[11] Simada Y and Sasa S. *Flight dynamics*. 1st edition, Morikita Publishing Co, 2017.

[12] Ishioka S, Uchiyama K and Masuda K. Optimal landing guidance for a fixed-wing UAV based on dynamic window approach. *American Institute of Aeronautics and Astronautics Scitech*, USA, 2019.

[13] McLean D. *Automatic flight control systems*. 2nd edition, Prentice Hall, 1990.

[14] The Japan Society for Aeronautical and Space Sciences. *Aerospace engineering handbook*. 3rd edition, Maruzen Publishing Co, 2005.

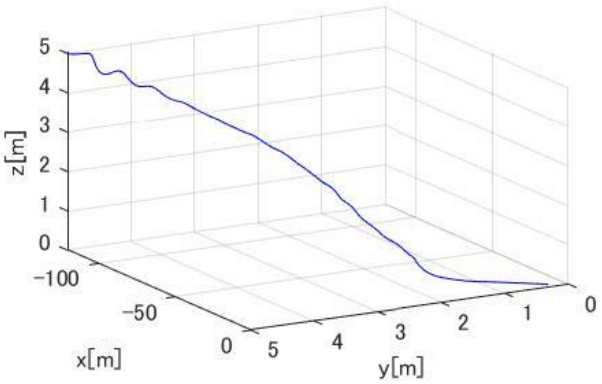

(a) Trajectory

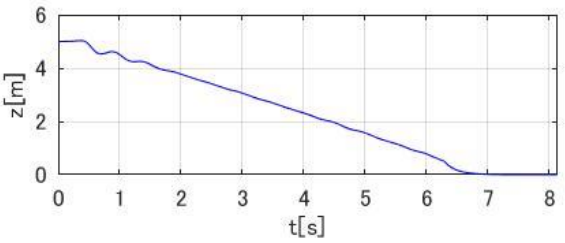

(b) Altitude

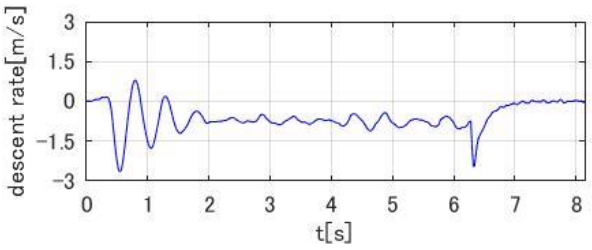

(c) Descent rate

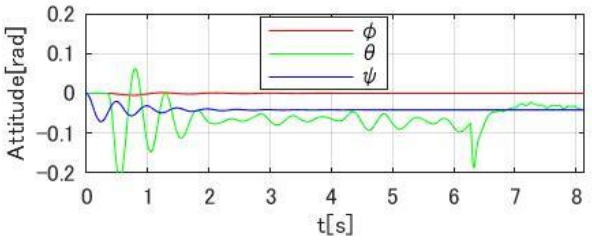

(d) Attitude

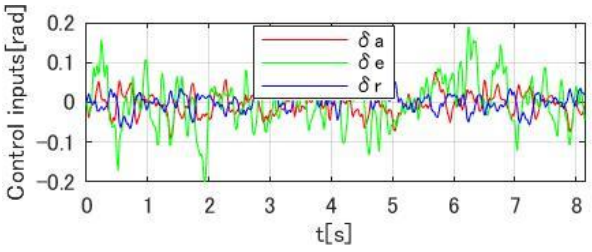

(e) Control inputs

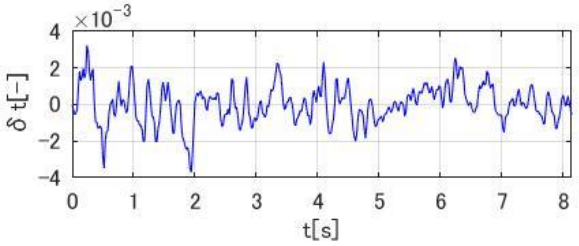

(f) Throttle

Figure 5 – G&F in condition 1.

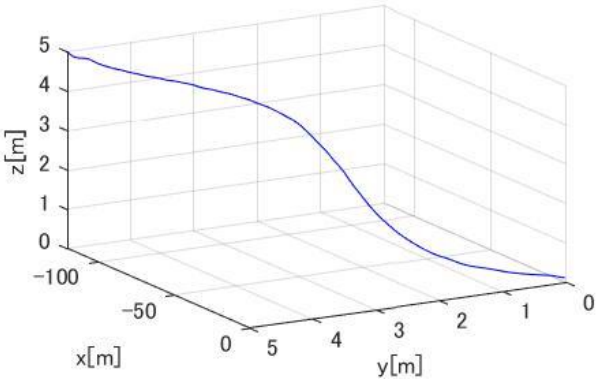

(a) Trajectory

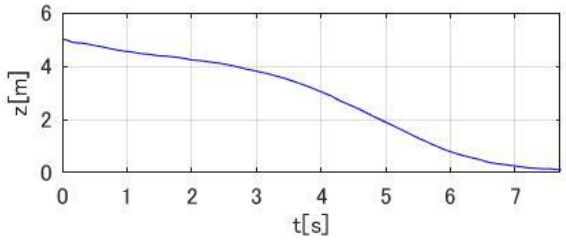

(b) Altitude

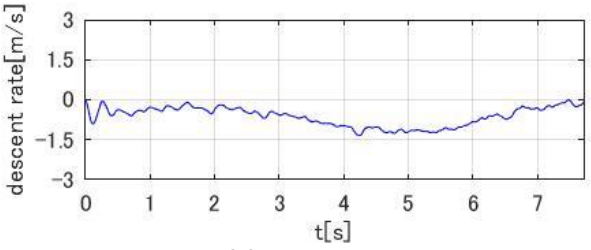

(c) Descent rate

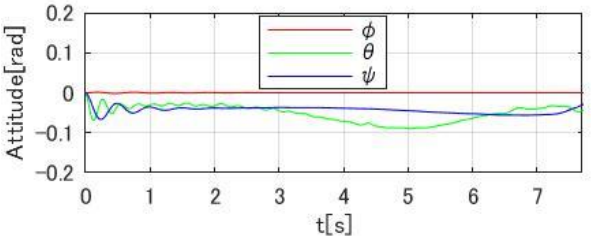

(d) Attitude

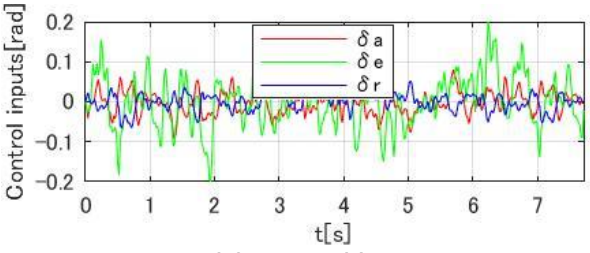

(e) Control inputs

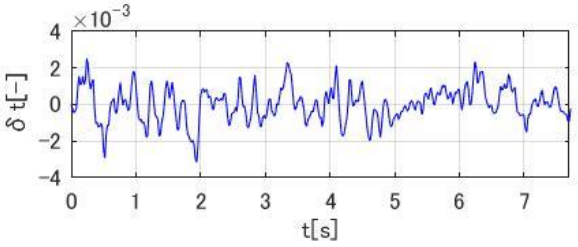

(f) Throttle

Figure 6 – EDWA in condition 1.

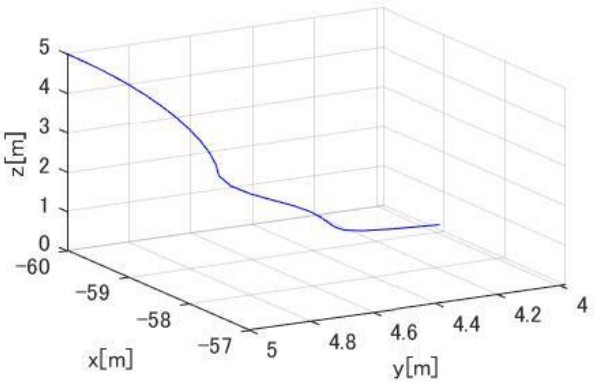

(a) Trajectory

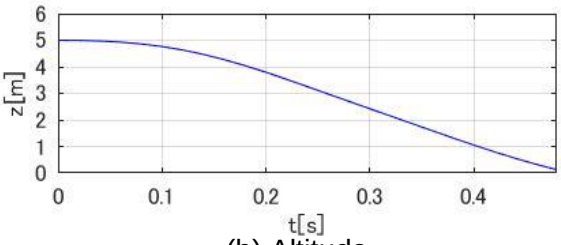

(b) Altitude

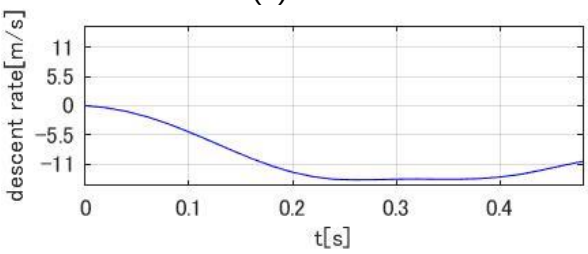

(c) Descent rate

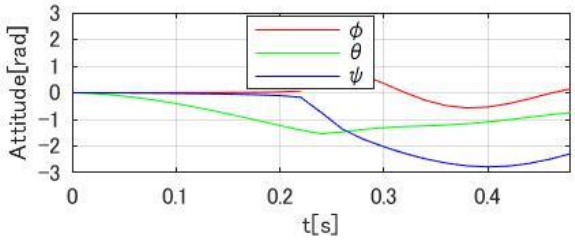

(d) Attitude

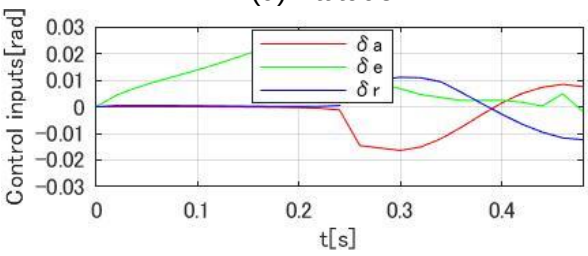

(e) Control inputs

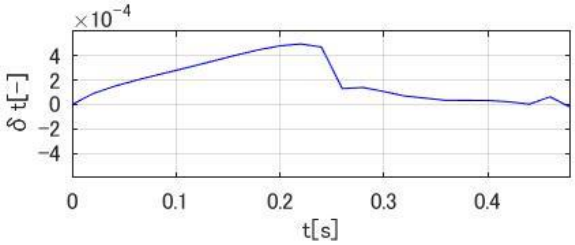

(f) Throttle

Figure 7 – G&F in condition 2.

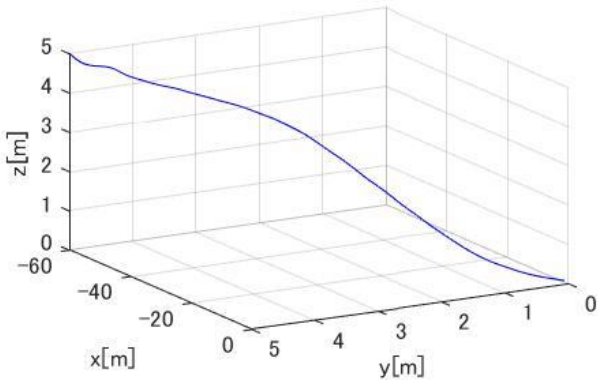

(a) Trajectory

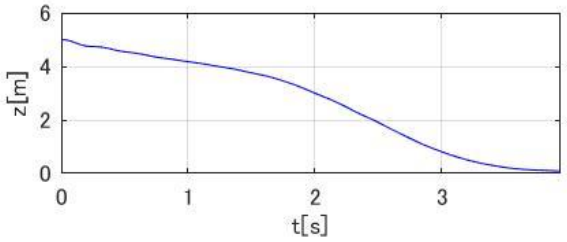

(b) Altitude

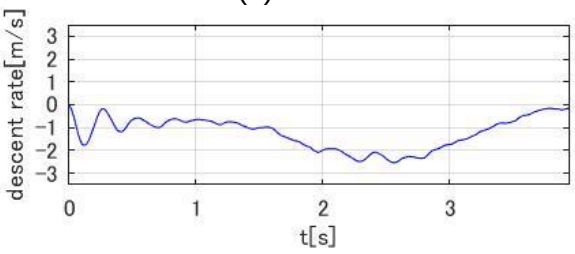

(c) Descent rate

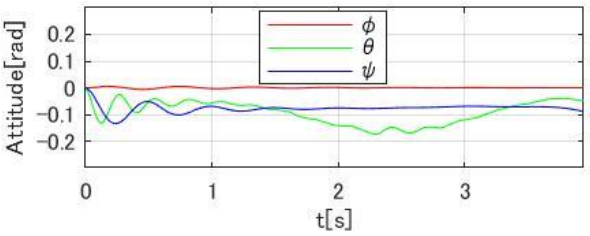

(d) Attitude

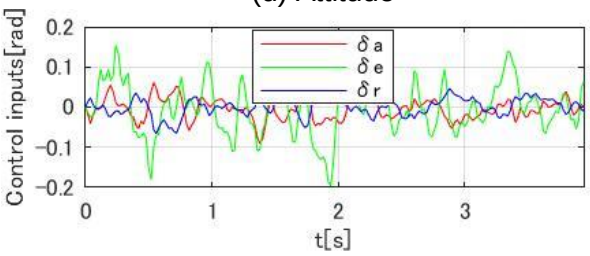

(e) Control inputs

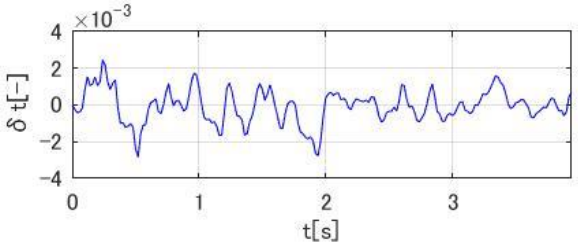

(f) Throttle

Figure 8 – EDWA in condition 2.

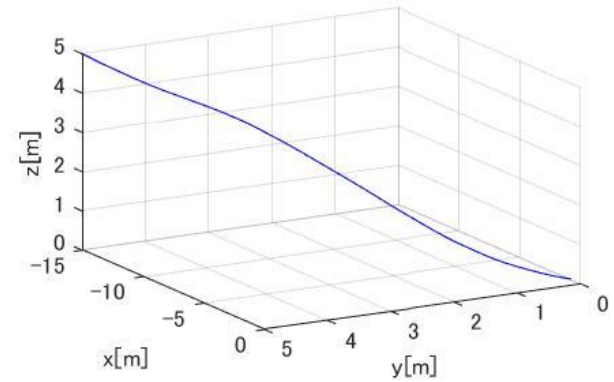

(a) Trajectory

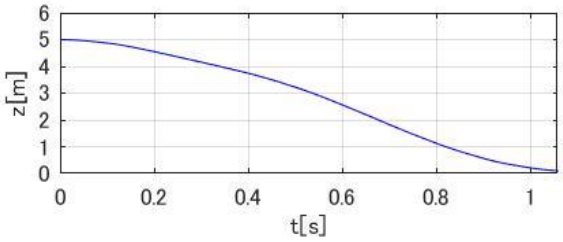

(b) Altitude

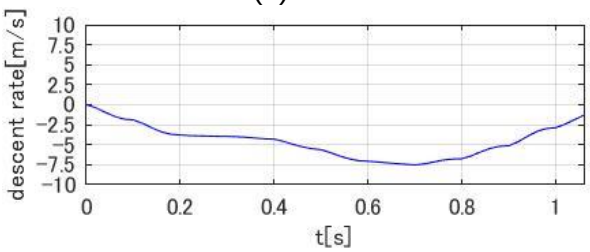

(c) Descent rate

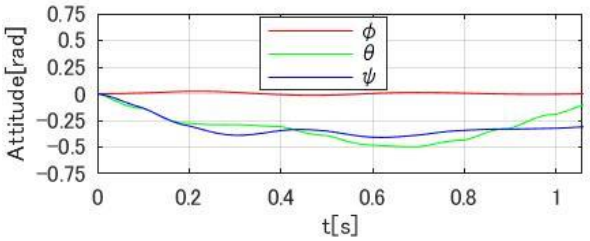

(d) Attitude

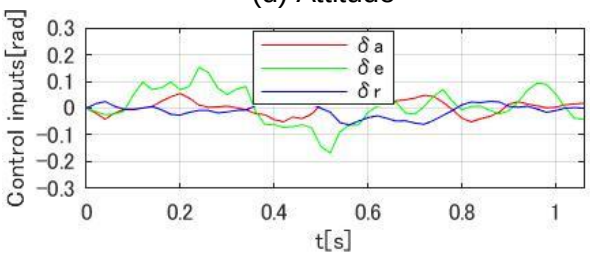

(e) Control inputs

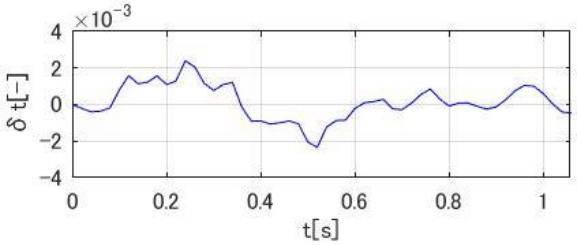

(f) Throttle

Figure 9 – Distance of possible landing

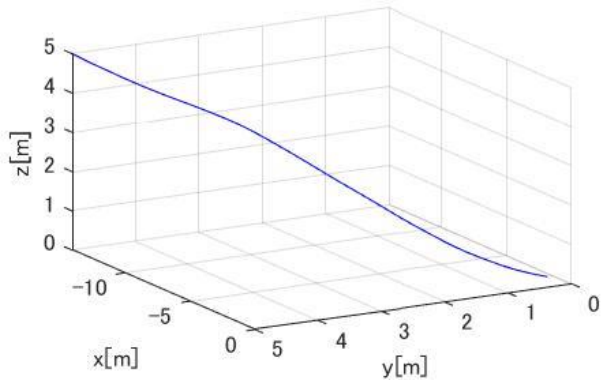

(a) Trajectory

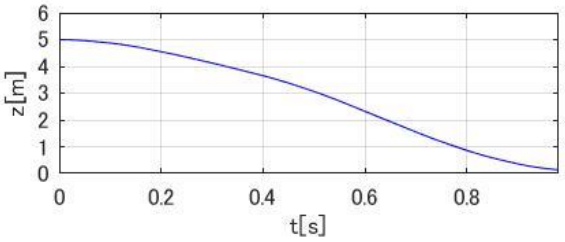

(b) Altitude

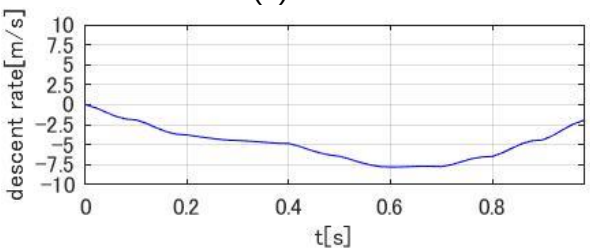

(c) Descent rate

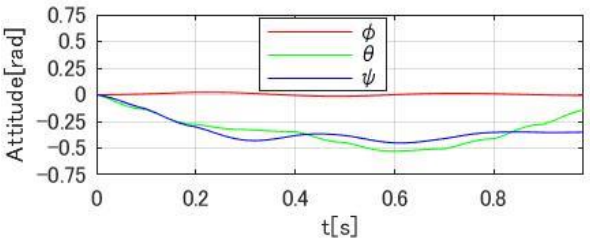

(d) Attitude

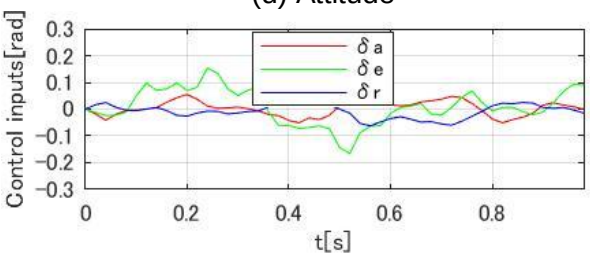

(e) Control inputs

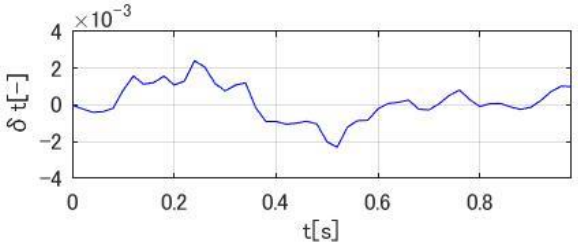

(f) Throttle

Figure 10 – Distance of impossible landing.